Supporting Information

Design of End-to-End Assembly of Side-Grafted Nanorods in a Homopolymer Matrix

Yulong Chen[1], Qian Xu[1], Yangfu Jin[1], Xin Qian[1]*, Li Liu[2], Jun Liu[2]*, and Venkat Ganesan[3]*

[1]College of Materials Science and Engineering, Zhejiang University of Technology, Hangzhou 310014, China

[2]Key Laboratory of Beijing City on Preparation and Processing of Novel Polymer Materials, College of Materials Science and Engineering, Beijing University of Chemical Technology, Beijing 100029, China

[3]Department of Chemical Engineering, University of Texas at Austin, Austin, Texas 78712, United States

*Corresponding author: qianx@zjut.edu.cn (X.Q.), liujun@mail.buct.edu.cn (J.L.), venkat@che.utexas.edu (V.G.)

I. Additional Phase Diagrams for Two Different Nanorod Concentrations

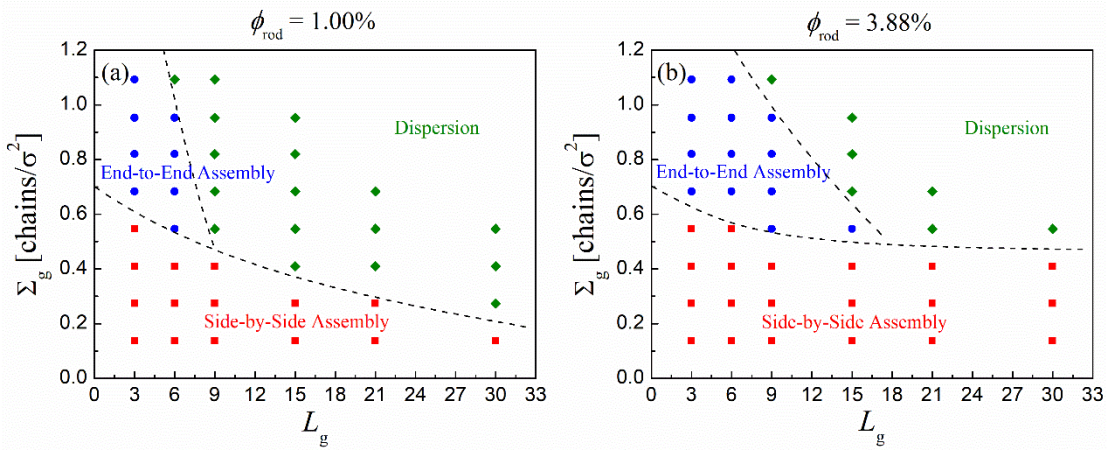

Figure S1. Phase diagrams in the L_g–Σ_g plane summarizing all the dominant structures obtained through simulations for two different nanorod (NR) concentrations ϕ_{rod} as indicated. The black dashed lines that separate different regions are merely guides to the eye.

From Figure S1, we can see that as ϕ_{rod} increases, the phase boundary between side-by-side aggregation to others and that between end-to-end assembly to dispersion are shifted toward higher grafting densities Σ_g and longer graft lengths L_g, respectively.

II. Dispersion State of Bare NRs in a Homopolymer Matrix

As shown in Figure S2, bare NRs tend to aggregate and form structures with local ordering in which the rods are aligned side-by-side.

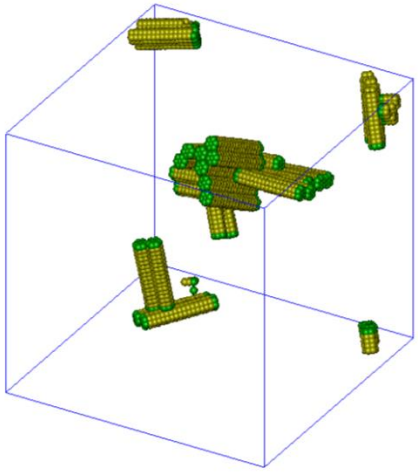

Figure S2. Snapshot shows the side-by-side aggregation of bare NRs in a homopolymer matrix.

III. Grafted Chain Architecture around NRs

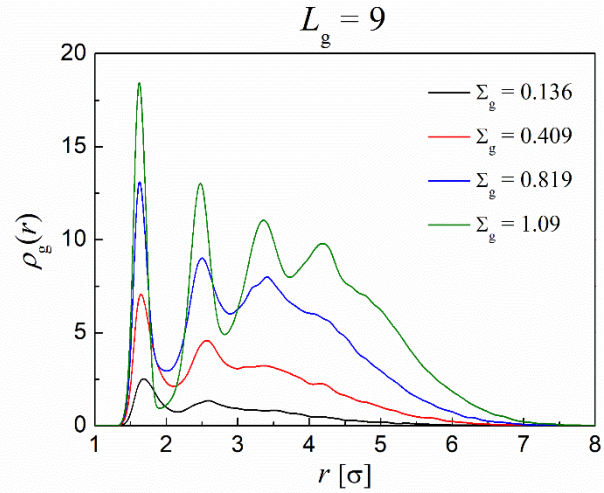

Figure S3. Bead number densities as a function of radial distance from the NR diametrical axis for the grafted chains that are tethered to the reference NR, $\rho_g(r)$, for the systems at $L_g = 9$ and at different grafting densities Σ_g as indicated.

Figure S3 indicates that the density profiles $\rho_g(r)$ of the grafted chains that are tethered to the reference NR show oscillatory behavior near the NR due to the finite bead size (σ),[1] while the profiles become smooth at larger distances from the NR.

Figure S4a shows the ratio of the mean-square radius of gyration of grafted chains over that of "unperturbed" grafted chains, i.e., if they were not grafted to the NR surface but were present free in the polymer matrix, $\langle R_g^2 \rangle / \langle R_{g,free}^2 \rangle$, which can indicate the change of chain configurations after they were grafted onto the NRs. We find that chain extension occurs for all values of L_g and Σ_g since the values of $\langle R_g^2 \rangle / \langle R_{g,free}^2 \rangle$ are larger than 1.0. With increasing Σ_g, the value of $\langle R_g^2 \rangle / \langle R_{g,free}^2 \rangle$ increases slowly below a threshold (designated as "critical grafting density $\Sigma_{g,c}$") and rapidly above $\Sigma_{g,c}$. We infer that this is the configurational transition of the grafted chains from mushroom to brush regimes. In the mushroom regime, i.e., at low grafting densities, the grafted chains have conformational freedom for sustaining their original random-coil,[2,3] and the slight extension of chains is partially due to the end-grafting effect. While in the brush regime,

i.e., when the grafting density beyond the critical value $\Sigma_{g,c}$, the grafted chains will be disturbed from their ideal random-walk state and stretch out to avoid each other as well as themselves.[2,3]

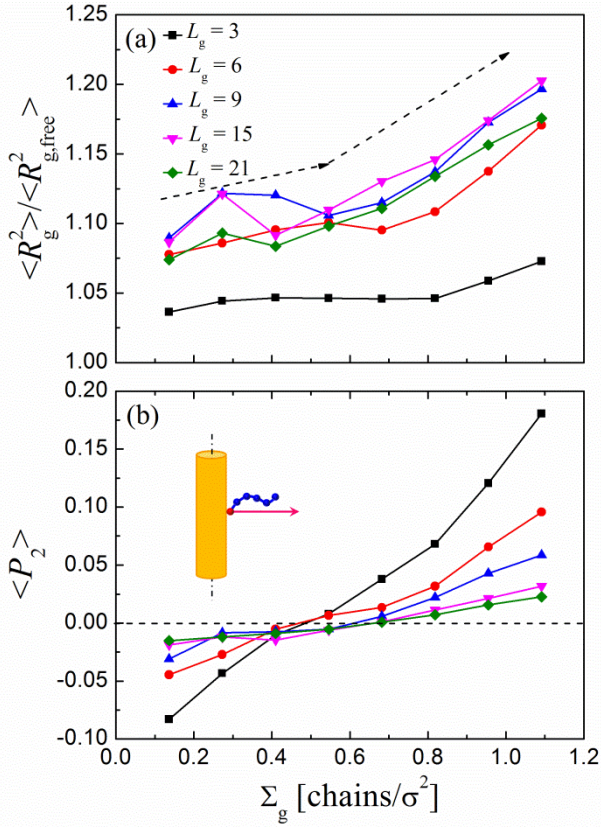

Figure S4. (a) Ratio of the mean-square radius of gyration of grafted chains over that of "unperturbed" grafted chains, $\langle R_g^2 \rangle / \langle R_{g,free}^2 \rangle$, and (b) average bond orientation of grafted chains along the direction normal to the grafting surface, $\langle P_2 \rangle$, as a function of grafting density Σ_g for different graft lengths L_g.

To further characterize the microstructures of the grafted chains, we also calculated the average bond orientation of the grafted chains along the direction normal to the grafting surface, i.e., the NR's radial direction, via the second Legendre polynomial $\langle P_2 \rangle$, also known as the Hermans orientation function, which is defined as follows:

$$\langle P_2 \rangle = \frac{1}{2}\left(3\langle \cos^2 \theta \rangle - 1\right) \quad \text{(S1)}$$

where θ is the angle between the bond vector of the grafted chains and the radial direction of the NRs. The order parameter $\langle P_2 \rangle$ has an upper bound at 1.0, which corresponds to a perfect alignment along the NR's radial direction, and a lower bound at –0.5, which represents bonds in the plane perpendicular to the radial direction. And $\langle P_2 \rangle$ = 0.0 indicates the bonds do not have any preferred orientation. The results are presented in Figure S4b, from which we can see that the bonds show a slight preference to align parallel to the grafting surface at low grafting densities, particularly when the grafted chains are short. The reason is that when the short chains are sparsely grafted onto the NRs, they prefer to twine around the NRs rather than mix with longer matrix chains because the gain in mixing entropy cannot overcome the loss of configurational entropy.[4] With increasing grafting density, the bonds gradually orient along the radial direction because the surface of the NRs becomes saturated, and hence the grafted chains tend to extend out to adjust the spatial position. At higher graft lengths, similar trends are also observed but much closer to zero for the entire range of grafting density. In this case, the matrix chains begin to penetrate into the grafted chains because the increase in mixing entropy of long, randomly oriented, grafted chains with the matrix now can compensate the loss of configurational entropy.

IV. Scaling Relation between the Grafted Polymer Thickness and Grafting Density

Theoretically, the thickness of grafted polymer in good solvents in the mushroom regime is independent of grafting density,[2] i.e., $h_g \sim (\Sigma_g)^0$. While in the present study, the sparsely grafted chains prefer to twine around the NRs rather than mix with the longer matrix chains because the gain in mixing entropy cannot overcome the loss of configurational entropy. With increasing grafting density, the grafted chains tend to extend out to adjust the spatial position. Therefore, the polymer height still exhibits a slight increasing trend with the increase of Σ_g in the mushroom

regime for all L_g (Figure 8) and hence the exponent $\beta = 0.116 \pm 0.011$ is larger than zero. In the brush regime, the relation between the brush height and grafting density becomes rather complicated, which is affected by various factors, such as the curvature of the NR surface, the grafted chain length, and the solvent/melt condition. According to the scaling theory, Binder and Milchev[5] predicted that for $R_{rod} \ll h_g$,

$$h_g \propto \left(\Sigma_g\right)^{\frac{1-\nu}{1+\nu}} \left(L_g\right)^{\frac{2\nu}{1+\nu}} \tag{S2}$$

While in the opposite limit $R_{rod} \gg h_g$, the grafted polymer on NR should be considered as a flat brush (the effect of NR surface curvature can be neglected at such high R_{rod}),

$$h_g \propto \left(\Sigma_g\right)^{\frac{1}{2\nu}-\frac{1}{2}} L_g \tag{S3}$$

where ν is the Flory exponent ($\nu = 1/2$ under athermal condition and $\nu = 3/5$ under good solvent condition). Here we take $\nu = 1/2$ since our simulation systems are composed of grafted NRs in an athermal polymer melt. Therefore, $h_g \sim (\Sigma_g)^{1/3}$ when $R_{rod} \ll h_g$ and $h_g \sim (\Sigma_g)^{1/2}$ when $R_{rod} \gg h_g$. As expected, the exponent values of β for the brushes at different L_g are located within the range from 1/3 to 1/2, as shown in Table 1, where the radius of the NRs ($R_{rod} = 1.17\sigma$) are comparable with the brush heights (Figure 8). Increasing chain length pushes the trend toward the theoretically predicted $(\Sigma_g)^{1/3}$ as h_g increases to about $6R_{rod}$.

V. Potential of Mean Forces between NRs

Figure S5a demonstrates that for the side-by-side aggregated systems, there are short-ranged attractions between the NRs which should be arisen from the intrinsic rod–rod attractions and the polymer-induced depletions. The oscillatory behavior of the potential of mean forces (PMFs) is

consistent with the results shown in Figure 3a. And the attractive potentials begin at approximately $r = D_{rod}$ indicates the preference of side-contact aggregation.

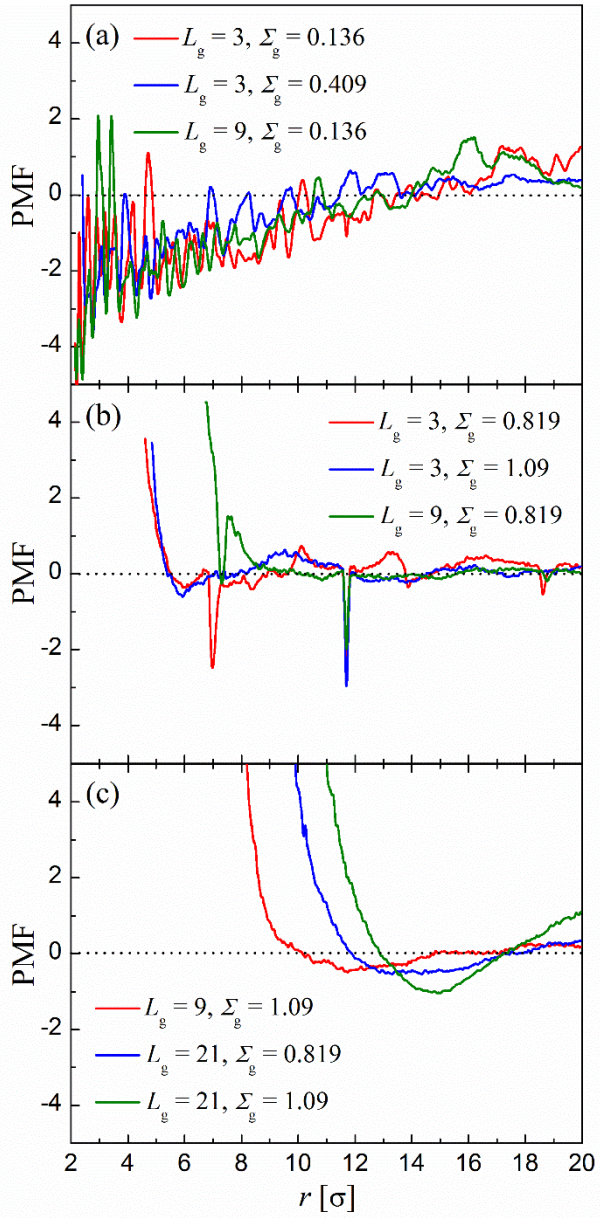

Figure S5. Potential of mean forces of several typical systems of (a) side-by-side aggregated, (b) end-to-end aligned, and (c) isolated dispersed NRs.

Figure S5b shows the results for the systems dominated by end-to-end assembly. From the figure, we observe a longer-ranged repulsion between the NRs (at $r > 4\sigma$) due to the steric hindrance arising from the polymer brushes. With increasing L_g or Σ_g, the repulsive distance

becomes larger, in line with the expectation that the longer or denser grafts offer increased steric stabilization.[6] At approximately $r = H_{rod}$, there is a sharp downward peak for all three example systems as indicated, demonstrating the existence of strong end–end attraction. As such, end-to-end alignment is preferred. Note that for the PMF at $L_g = 3$ and $\Sigma_g = 0.136$ chains/σ^2, an attraction also appears at about $r = 7\sigma$ due to the end-to-side connection of part NRs, a phenomenon typically exists in the systems located near the boundary between the side-by-side and end-to-end phases (Figure S6).

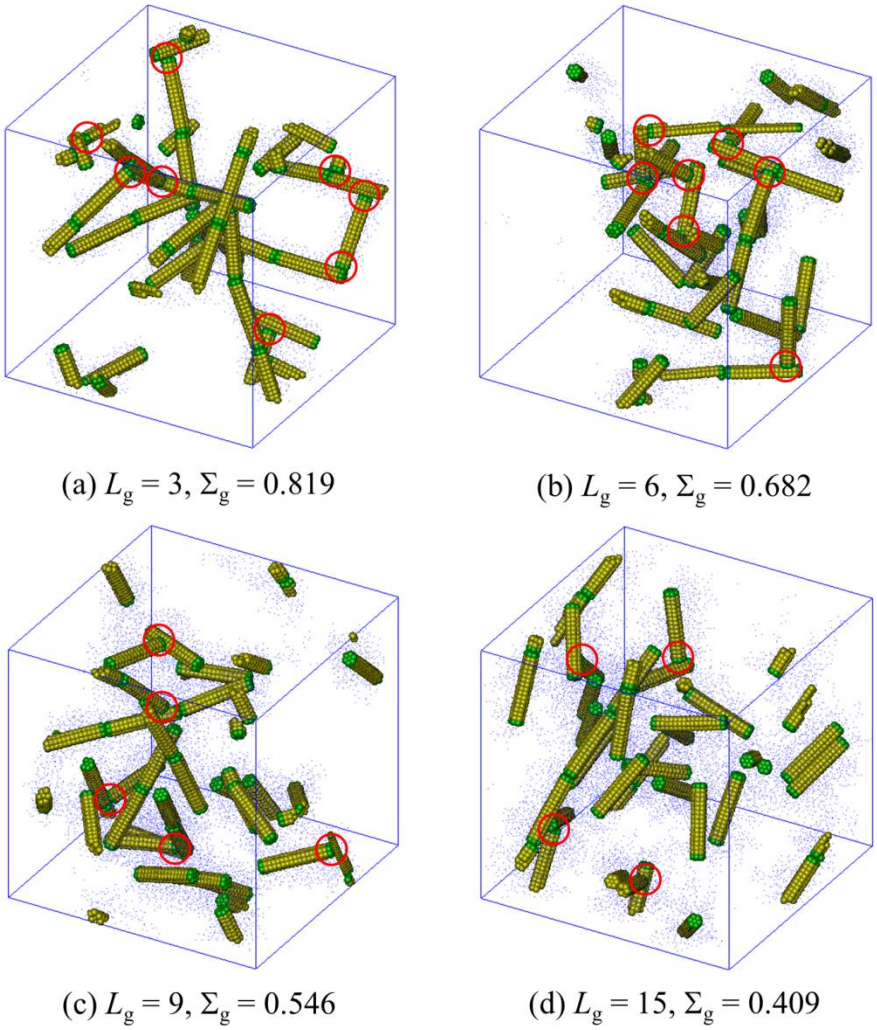

Figure S6. Snapshots for some typical systems located near the mushroom-to-brush crossover. Red cycles identify the end-to-side connections of NRs. It can be observed that the NRs mainly assemble end-to-end, but there also some NRs connect end-to-side.

In Figure S5c, we display PMFs for the systems of isolated dispersed NRs. Again, we observe steric repulsions between the NRs with distances much farther than those observed from Figure S5b. Similarly, the repulsive distance also increases with increasing L_g or Σ_g. Different from Figure S5b, in the present figure, the sharp peak at $r = H_{rod}$ is absent. These results indicate that the NRs prefer to remain isolated in the matrix. Note that these PMFs also have a weakly attractive minimum. The depth and position of the attractive well depend significantly on Σ_g. With increasing Σ_g, the attractive well becomes deeper. The exclusion of the matrix chains from the brush at high enough grafting density, i.e., the well-known autophobic dewetting,[4] is responsible for this attractive well, which may lead to a slight aggregation of the brush-coated NRs. Since such aggregation is weak and separated by the coated polymer brushes, in this study, we still considered these particles as isolated dispersed NRs.

VI. The Formation of Liquid Crystalline Structure of NRs

Figure S7 shows that the NRs densely grafted with short chains can self-organize into liquid crystalline structure at high ϕ_{rod} in addition to their end-to-end assembly. Figure S8 presents the results of the local rod alignment as a function of the distance between NR long axes, as measured by the second Legendre polynomial $P_2(r) = (3\langle cos^2\theta\rangle - 1)/2$, where θ is the angle between rods at distance r, which reveals very weak parallel orientational correlations at low ϕ_{rod} but significant local ordering at high ϕ_{rod}, persisting over relatively large distances.

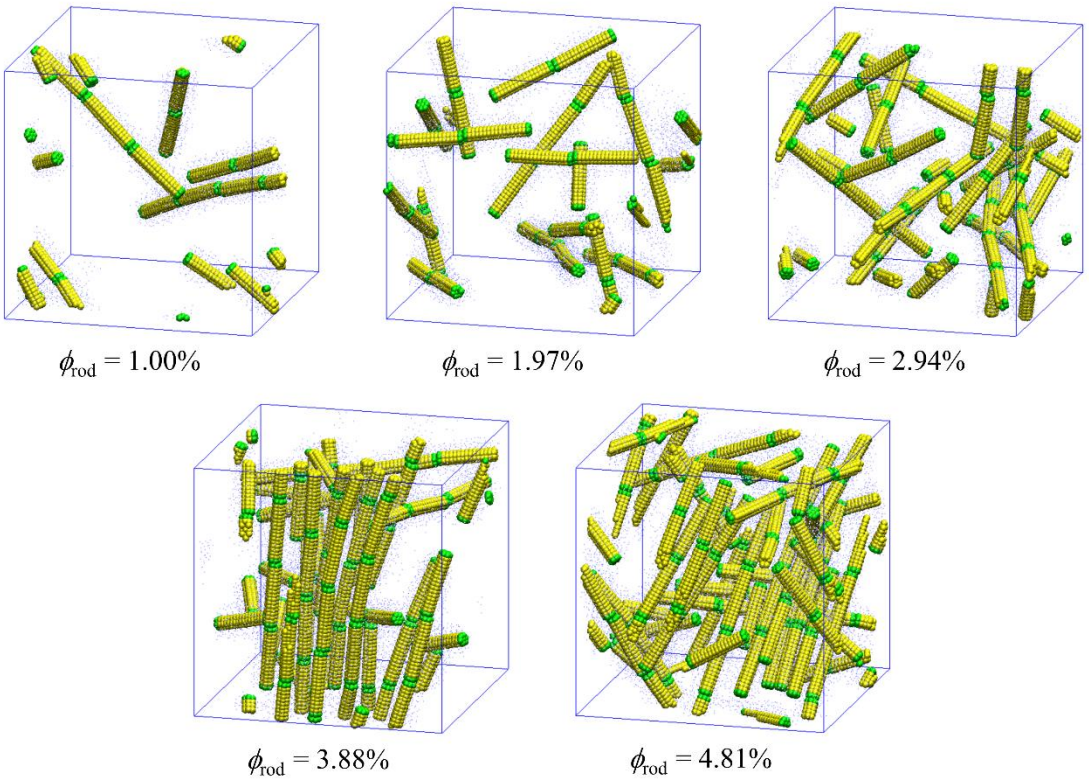

Figure S7. Simulation snapshots of the typical structures formed by the NRs densely grafted with short chains (Σ_g = 1.09 chains/σ^2 and L_g = 3) at different NR volume fractions ϕ_{rod} as indicated.

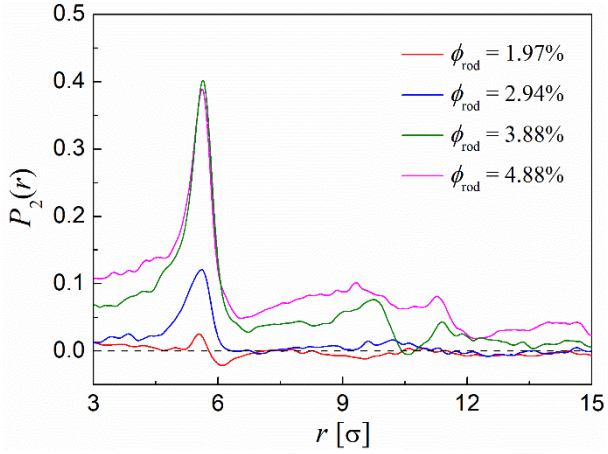

Figure S8. The second Legendre polynomial as a function of the distance between NR long axes. Averaged over a set of rod pairs, this value is –0.5 for perpendicular alignment, 1.0 for parallel alignment, and 0.0 for random alignment. Results are shown for different ϕ_{rod} but at fixed Σ_g = 1.09 chains/σ^2 and L_g = 3.

VII. Additional Results for the Effect of NR Aspect Ratio

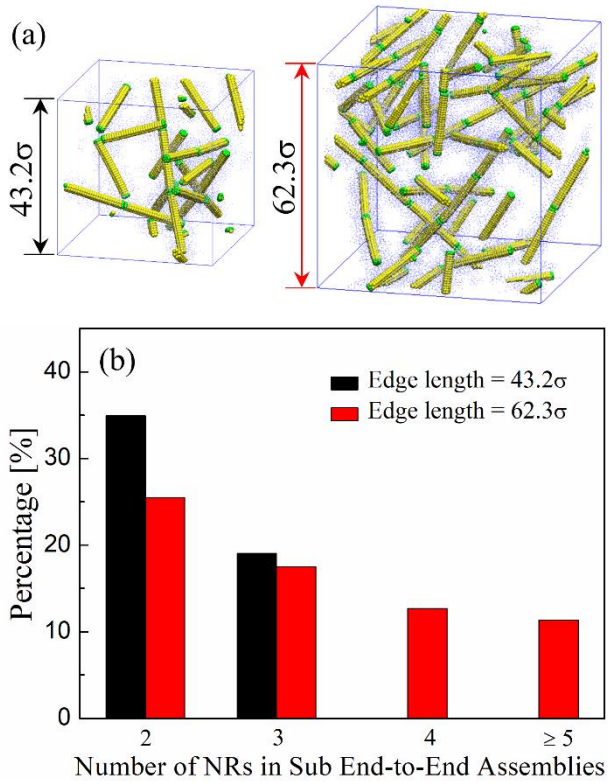

Figure S9. (a) Simulation snapshots and (b) percentages of the NRs that align in end-to-end assemblies having two, three, four, or more NRs, shown for different box sizes as indicated. The results are for $S = 7.57$, $\phi_{rod} = 1.97\%$, $L_g = 6$, and $\Sigma_g = 0.819$ chains/σ^2.

In the simulations for the effect of NR aspect ratio, the boxes are of edge lengths equal to 43.2σ which is about 2.45 times that of the length of the NRs for the highest aspect ratio (S = 7.57) examined in this study. To check the finite size effect, a simulation, containing 201600 polymer beads and 60 NRs in the box with edge lengths of 62.3σ (3.53 times that of the NR length), was conducted. It is found that the simulations with different box sizes produce similar structures with the exceptions that the NRs in larger box show the ability to self-organize into much longer end-to-end configurations (containing four or even more NRs in the sub-assemblies), and overall the total percentage of the end-to-end assembly is also slightly increased,

as shown in Figure S9. These results indicate that the finite box size effect may be a partial reason for the reduction of end-to-end alignment of NRs of high aspect ratio.

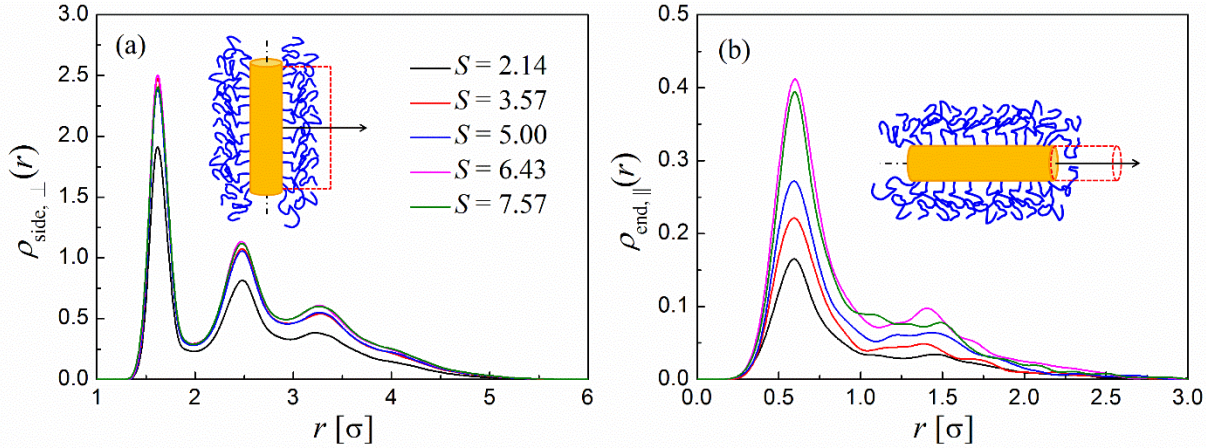

Figure S10. Bead number density profiles of the grafted chains (a) perpendicular to the NR sides, $\rho_{\mathrm{side},\perp}(r)$, and (b) those taken at the surface of the NR ends along the axial direction, $\rho_{\mathrm{end},\parallel}(r)$, for the systems of different NR aspect ratios S as indicated.

For the role of brush comb over, we show in Figure S10a that at low NR aspect ratio (S = 2.14), the comb over of the polymer brush would reduce the effective grafting density on the NR sides. With increasing NR length, the brush comb over shows less influence on the effective side grafting density. However, the more crowding side brush at higher S in turn would enhance the splaying of the grafted chains over the bare ends, as shown in Figure S10b.

We have also monitored the self-assembly processes of NRs of both low and high aspect ratios (i.e., S = 3.57 and 7.57, respectively). The results are shown in Figure S11. It can be found that in both cases, the percentages of end-to-end assembly show a step-by-step jump increasing trend until to a constant value with the increase of simulation time. However, the high aspect ratio NRs are assembled slower than that of low aspect ratio, confirming that the slower rotation kinetics of high aspect ratio NRs may also be a likely reason trapped their self-assembly.

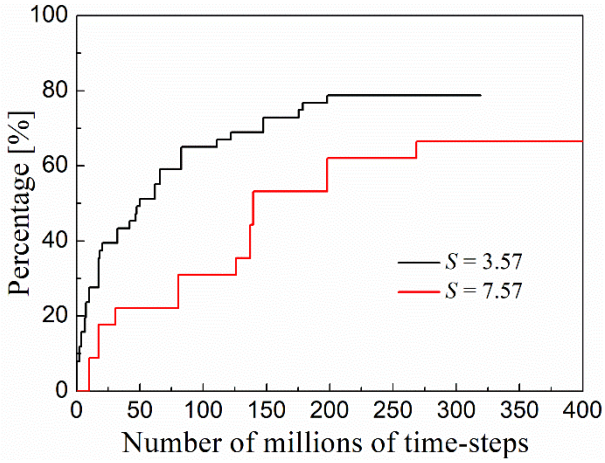

Figure S11. Percentages of end-to-end alignment as a function of time for systems of two different NR aspect ratios S as indicated. The results are for ϕ_{rod} = 1.97%, L_g = 6, and Σ_g = 0.819 chains/σ^2.

References

(1) Frischknecht, A. L.; Hore, M. J.; Ford, J.; Composto, R. J. Dispersion of Polymer-Grafted Nanorods in Homopolymer Films: Theory and Experiment. *Macromolecules* **2013**, *46*, 2856–2869.

(2) Wu, T.; Efimenko, K.; Genzer, J. Combinatorial Study of the Mushroom-to-Brush Crossover in Surface Anchored Polyacrylamide. *J. Am. Chem. Soc.* **2002**, *124*, 9394–9395.

(3) Chen, W. L.; Cordero, R.; Tran, H.; Ober, C. K. 50th Anniversary Perspective: Polymer Brushes: Novel Surfaces for Future Materials. *Macromolecules* **2017**, *50*, 4089–4113.

(4) Reiter, G.; Khanna, R. Negative Excess Interfacial Entropy between Free and End-Grafted Chemically Identical Polymers. *Phys. Rev. Lett.* **2000**, *85*, 5599–5602.

(5) Binder, K.; Milchev, A. Polymer Brushes on Flat and Curved Surfaces: How Computer Simulations Can Help to Test Theories and to Interpret Experiments. *J. Polym. Sci. Part B: Polym. Phys.* **2012**, *50*, 1515–1555.

(6) Striolo, A.; Egorov, S. A. Steric Stabilization of Spherical Colloidal Particles: Implicit and Explicit Solvent. *J. Chem. Phys.* **2007**, *126*, 014901.